American Mineralogist, Volume 81, pages 864–873, 1996

Chemical state of Cd in apatite phosphate ores as determined by EXAFS spectroscopy

ANNE SERY,[1] ALAIN MANCEAU,[1] AND G. NEVILLE GREAVES[2,3]

[1]Environmental Geochemistry Group, LGIT-IRIGM, University of Grenoble and CNRS, BP 53, 38041 Grenoble cedex 9, France
[2]DRAL Daresbury Laboratory, Warrington WA4 4AD, U.K.
[3]Geoscience Research Institute, University of Manchester, Manchester M13 9PL, U.K.

ABSTRACT

Natural apatites used in fertilizer industries often contain trace amounts of Cd, which may reach concentrations of several tens to a few hundred parts per million. Cd is not eliminated during the production of phosphate fertilizers, and its concentration in the final product can exceed environmental norms. Knowledge of the chemical state of Cd in apatite ores is a prerequisite for the design of technical processes of extraction. In the present study, Cd *K*-edge EXAFS spectroscopy was used to investigate the structural environment of Cd present in sedimentary apatite ores from West Africa. These apatites are fluorinated and contain goethite, quartz, and crandallite as ancillary phases detected by X-ray diffraction or EXAFS spectroscopy. Cd *K*-edge EXAFS spectra for two natural samples were analyzed and compared with those for Cd-containing reference minerals, including hydroxylapatite, goethite, otavite, and crandallite. A good spectral resemblance was observed between natural products and synthetic apatite containing small amounts of Cd. This spectral likeness indicates that the majority of Cd atoms are diluted in the apatitic framework and do not form $Cd_{10}(PO_4)_6(OH,F)_2$ clusters. This finding was confirmed by quantitative analysis of the EXAFS spectra, which indicated that Cd atoms are surrounded by nearest O atoms at 2.33 Å, next-nearest P atoms at ~3.53 Å, and a third-nearest shell of Ca atoms at ~4.02 Å. A comparison of these data with those obtained for synthetic apatites allowed us to assess that Cd occupies both Ca crystallographic sites with a slight preference for the Ca2 site.

INTRODUCTION

Cd is one of several metals that have come under suspicion within the last 20 years as an environmental contaminant potentially harmful to human health. Cd accumulates in the liver and kidney, increasing over the course of a lifetime, and can lead to various disorders such as kidney disfunction (Thomas and Spiro 1994). The main risks of Cd do not originate from industrial products containing Cd but from its diffuse dispersion into the environment caused by atmospheric deposition in the vicinity of nonferrous metal smelters, soil application of municipal sewage sludge, and phosphate fertilizers (Nriagu 1980; Thomas and Spiro 1994). Many phosphate ores contain Cd in amounts ranging from several tens to a few hundred parts per million (Williams 1974), most or all of which is not eliminated during phosphate fertilizer production (Williams and David 1976; Hutton 1983). The Cd content of soils is gradually rising because of phosphate amendments. Studies have shown that Cd is fairly mobile in soils and bioavailable (Mortvedt and Osborn 1982); thus, a rise in the Cd level of soils increases the likelihood of uptake by plants. In addition, because the primary source of Cd contamination of living organisms is consumption of vegetables, Cd intakes by human beings are also increasing (de Boo 1990). The use of Cd-free phosphate fertilizers would decrease the accumulation rate of Cd in soils. Production of Cd-free phosphate fertilizers requires removal of Cd from phosphate ores during their transformation. Obtaining a basic knowledge of the crystal chemistry of Cd in phosphate ores is a prerequisite for designing technical extraction processes. Several possibilities can be envisaged for the location of Cd: substitution or insertion in the apatitic framework or in ancillary phases, precipitation of a pure Cd-bearing phase such as cadmium carbonate (Stipp et al. 1992) or Cd–end-member apatite, or sorption on mineral surfaces. Because of the low concentration of Cd in natural phosphate rocks, the determination of its chemical state is experimentally very difficult and has not yet been achieved.

Fluorescence-yield extended X-ray absorption fine-structure (EXAFS) spectroscopy is one of the very few methods capable of selectively probing the structural environment of a diluted atom and is particularly suited for determining the speciation of trace metals in chemically and structurally complex solids. The EXAFS method was used in the present study to examine the chemical state

0003–004X/96/0708–0864$05.00

of Cd in natural phosphate ores. EXAFS spectroscopy consists of recording and analyzing the variations of the absorption coefficient above an absorption edge for a given element (Teo 1986; Koningsberger and Prins 1988). Variations in the absorption coefficient originate from interferences between the outgoing electronic wave from the X-ray absorber and the incoming wave that is backscattered by the electrons of neighboring atoms (backscatterers). Analysis of the absorption modulations provides structural information concerning the local environment of the target atom, or absorber (i.e., Cd), in terms of interatomic distances and the type and number of neighboring atoms in the two to three nearest atomic shells. Thus, EXAFS spectroscopy has the potential to differentiate the various possible structural solutions previously envisaged for the location of Cd in phosphate ores.

Two samples from West Africa were collected for study at two stages in the treatment of phosphate ore. Despite the low concentration of Cd in these samples (90–100 ppm), the quality of EXAFS spectra was high enough to determine the crystallographic site location of Cd atoms. To help in this determination, the structural environment of Cd atoms in various minerals, including synthetic hydroxylapatite containing various amounts of substitutional Cd, as well as Cd-containing goethite (α-FeOOH) and otavite ($CdCO_3$), was also investigated.

Materials

Reference samples

Three synthetic apatite phases were studied: $Cd_{10}(PO_4)_6OH_2$ (R1), $Ca_{9.5}Cd_{0.5}(PO_4)_6OH_2$ (R2), and $Ca_{9.995}Cd_{0.005}(PO_4)_6OH_2$ (R3). Hydroxylapatite [$Ca_{10}(PO_4)_6OH_2$] crystallizes in the hexagonal system with the space group $P6_3/m$ (a = 9.424, c = 6.879 Å) (Kay et al. 1964). Ca^{2+} ions occupy two crystallographic sites, Ca1 and Ca2 (Fig. 1). The former is on a threefold axis at x = ⅓, y = ⅓ (position 4f), and the latter is on a mirror at z = ¼ or z = ¾ (position 6h). Ca1 atoms are surrounded by nine O atoms, six at 2.43 Å and three at 2.80 Å. Ca2 atoms are surrounded by eight O atoms (seven at 2.41 Å and one at 2.71 Å, Table 1). In fluorapatite, F does not occupy the same crystallographic site as OH in hydroxylapatite. F atoms are found in channels along the hexagonal screw axes at z = 0.25 (Beevers and McIntyre 1945), whereas OH groups are located 0.3 Å away from the z = ¼ mirror. Ca1 possesses the same structural environment as in hydroxylapatite, but Ca2 atoms are surrounded by six O atoms (five at 2.41 Å and one at 2.69 Å) and one F atom (at 2.30 Å), making the Ca2 site slightly smaller than the Ca1 site (Fig. 1, Table 1). In apatites, interatomic distances are distributed, and the resolution of EXAFS is not high enough to differentiate all elementary distances associated with the various atomic pairs. Consequently, atoms of the same nature, and for which distances from the central Ca or Cd atom differ by <0.2 Å, were grouped in the same atomic shell. The distance reported in Table 1 for each atomic shell is thus an average of the elementary distances corresponding to all the atoms grouped within this shell. Examination of Table 1 reveals that in the Ca2 site (Ca,Cd)-P distances are shorter by 0.1 Å and (Ca,Cd)-(Ca,Cd) distances are longer by 0.1 Å, in comparison with the Ca1 site. Cd was shown, by diffraction studies, to substitute for Ca in both crystallographic sites but with a slight preference for the Ca2 site in the case of hydroxylapatite and for the Ca1 site in the case of fluorapatite at low substitution (Nounah et al. 1990, 1992; Jeanjean et al. 1994).

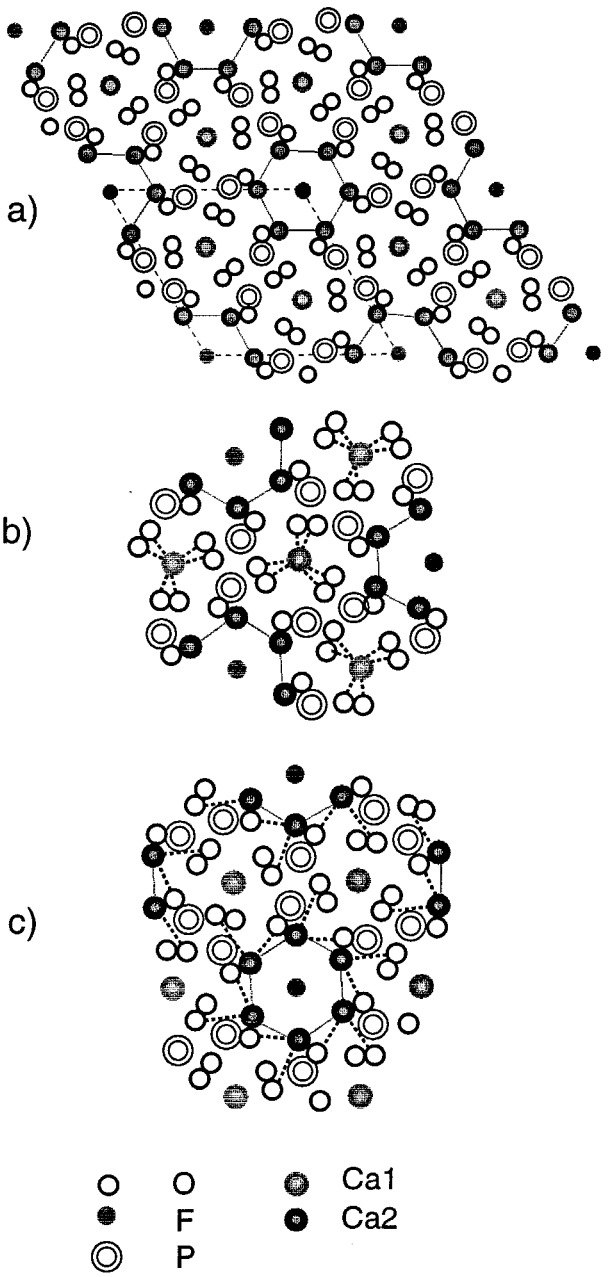

FIGURE 1. (a) Projection of the fluorapatite structure along the c axis (Beevers and McIntyre 1945). (b) Structural environment of Ca1. (c) Structural environment of Ca2.

TABLE 1. Structural environment of Ca and Cd for various hydroxyl- and fluorapatites as determined by diffraction data

Atom (X)*	CN	$Ca_{10}(PO_4)_6(OH)_2$** ⟨d(Ca-X)⟩ (Å)	$Ca_{10}(PO_4)_6(OH)_2$† ⟨d(Ca-X)⟩ (Å)	$Cd_{10}(PO_4)_6(OH)_2$‡ ⟨d(Cd-X)⟩ (Å)	CN	$Ca_{10}(PO_4)_6(F)_2$§ ⟨d(Ca-X)⟩ (Å)
			Ct1			
O	6	2.43	2.43	2.38	6	2.42
O	3	2.80	2.79	2.82	3	2.80
P1	3	3.21	3.21	3.21	3	3.20
Ct	2	3.44	3.44	3.33	2	3.44
P2	3	3.60	3.59	3.51	3	3.58
O	3	3.93	3.93	3.87	3	3.91
Ct	6	3.99	3.99	3.95	6	4.00
O	6	4.07	4.06	4.02	6	4.06
			Ct2			
F	—	—	—	—	1	2.30
O	7	2.41	2.41	2.41	5	2.41
O	1	2.71	2.70	2.64	1	2.69
P1	1	3.08	3.09	3.06	1	3.06
P2	4	3.52	3.54	3.45	4	3.53
O	3	3.97	3.98	3.91	—	—
Ct	10	4.08	4.08	4.00	10	4.05
F	—	—	—	—	2	4.14
O	7	4.43	4.44	4.38	7	4.40

* Atoms were grouped in coordination shells, and interatomic distances from the central atom were averaged.
** Hydroxylapatite from Holly Springs; X-ray and neutron diffraction. After Sudarsanan and Young (1969).
† Human tooth enamel; convergent-beam electron diffraction. After Brès et al. (1993).
‡ Synthetic Cd–end-member hydroxylapatite; X-ray diffraction. After Hata et al. (1978).
§ Fluorapatite. After Mackie and Young (1973).

Natural samples

The natural apatites were from sedimentary phosphate ore deposits located in West Africa. Sample S1 was a raw material and contained some clay, crandallite (aluminum phosphate), and quartz impurities as detected by X-ray diffraction. These major impurities were partially removed in sample S2 by granulometric, washing, and centrifugation treatments. The mineralogic nature of the main constituent was determined by X-ray diffraction and chemical analyses (Table 2) to be apatite. The concentration of F in these phosphates is particularly high (2.81%), and to determine its amount in the apatite structure, unit-cell parameters were refined. Least-squares refinement of *hkl* reflections led to $a = 9.367$ and $c = 6.881$ Å for the unit cell. By comparing these values with those of hydroxylapatite ($a = 9.424$ and $c = 6.879$ Å; Sudarsanan and Young 1969) and fluorapatite ($a = 9.367$ and $c = 6.884$ Å; Mackie and Young 1973), and taking into account the precision of the evaluation of the unit-cell parameters (~0.005 Å), we concluded that at least 90% of the natural apatite was fluorinated. The remaining 10% essentially consists of chlorapatite. The nature of the Fe-containing phase, as determined by fluorescence-yield Fe *K*-edge EXAFS spectroscopy, was found to be goethite (α-FeOOH).

TABLE 2. Chemical analysis of sample S2

	Wt%
CaO	47.70
P_2O_5	35.84
SiO_2	7.06
Al_2O_3	0.93
Fe_2O_3	0.94
Na_2O	0.07
MgO	0.03
K_2O	0.02
MnO	0.05
SrO	0.07
Li_2O	0.03
BaO	0.01
CdO	0.01
CO_2	0.10
SO_3	0.04
H_2O*	3.01
Cl	0.80
F	2.81
Total	99.52

Note: Sample S2 is a natural polyphase material composed of $Ca_{10}(PO_4)_6(OH,Cl,F)_2$, FeOOH, and SiO_2.
* Evaluated by weight loss at 1000 °C.

EXPERIMENTS AND DATA REDUCTION

Data collection

Samples were ground and placed in a sample holder, the thickness of which was adjusted from 1 to 10 mm depending on the concentration of Cd in the material and detection mode. X-ray absorption spectra were collected at ambient temperature on wiggler magnet beamlines 9.2 and 9.3 at the DRAL Synchrotron Radiation Source (SRS) at Daresbury, Warrington (U.K.). The electron storage ring operated at 2 GeV with an average beam current of ~200 mA. An Si(220) double-crystal monochromator was used. Higher harmonic reflections were rejected by detuning the primary beam by 30–50%. The spectrometer was calibrated using a cadmium metallic foil. Gas-ionization chambers were filled with an argon and helium mixture to attenuate the beam intensity by 20% before and 80% after the samples for transmission-mode measurements. Synthetic samples (R1, R2, and $CdCO_3$) were

measured in transmission mode. Spectra for diluted samples (R3, S1, S2, and α-FeOOH) were collected in fluorescence mode using a 13-element Ge array detector with a Be window. Multiple scans (three to eight depending on Cd concentration) were collected and averaged for each sample to improve the signal-to-noise ratio.

Data reduction

X-ray absorption spectra were treated following a standard procedure (Teo 1986). Cd K-edge EXAFS spectra were derived from raw absorption spectra by normalization to the atomic absorption jump. The kinetic energy of the photoelectron was converted into the modulus of the wave vector **k** to obtain the $\chi(k)$ function. This function is the summation of the elementary contributions to the EXAFS spectra of the very first atomic shells surrounding Cd. The atomic pair-correlation function, or radial distribution function (RDF), was obtained by Fourier transformation of $k^n\chi(k)$ spectra to real space using a Kaiser apodization window (Manceau and Combes 1988).

Structural parameters, namely interatomic distance (R) and coordination number (CN), characterizing the atomic environment of Cd atoms were determined by spectral simulations. These simulations require the knowledge of phase-shift and amplitude functions for each atomic pair under consideration. Two possibilities exist for evaluating these functions (Teo 1986). The first consists of determining empirical functions from a reference sample for the desired Cd-backscatterer pair. This procedure can be accurately applied if the contribution to EXAFS by the atomic pair can be isolated from the reference spectrum by Fourier transformation. But this is often impossible because of overlap of the various atomic shells in solids, or the lack of material or compound containing the atomic pair in question. The second possibility consists of using theoretical phase-shift and amplitude functions, which can be calculated with a program that models the interaction potential between the various atoms or which can be taken from tabulated values. The theory of EXAFS was extensively discussed by Lee and Pendry (1975). Their exact curved-wave theory is, however, mathematically complex and computationally time-consuming. This theory was simplified, among others, by Gurman et al. (1984). Their rapid curved-wave theory is coded analytically in the EXCURV suite of programs and enables multiple-shell fitting to raw EXAFS spectra using least-squares methods. More recently, McKale et al. (1988) calculated the amplitude and phase-shift functions for nearly every element in the periodic table by using a curved-wave formalism. These functions can be used by classical programs for EXAFS analysis. FITEX (homemade software) was employed in the present study in which atomic shells that were Fourier filtered from the EXAFS spectra were separately fitted.

Phase-shift and amplitude functions associated with Cd-O and Cd-Cd pairs were isolated from β-$Cd(OH)_2$

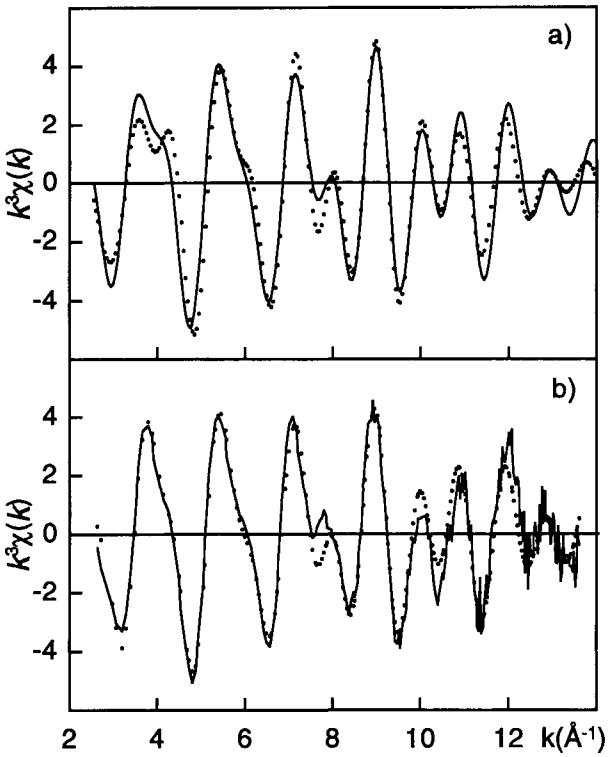

FIGURE 2. (**a**) Fourier-filtered Cd-O and Cd-Cd contributions to EXAFS for β-$Cd(OH)_2$ (solid line) fitted with theoretical spectrum (dotted line) using McKale's functions. (**b**) Whole EXAFS spectrum for β-$Cd(OH)_2$ (solid line) fitted with theoretical spectrum (dotted line) using the rapid curved-wave theory.

(Wyckoff 1971). But no reference compound was found to exist for Cd-P and Cd-Ca pairs. Because theoretical phase-shift and amplitude functions can be inaccurate, two sets of theoretical functions were used to simulate EXAFS spectra: (1) McKale's functions and (2) functions generated by the EXCURV suite of programs. The validity of Cd-O and Cd-Cd theoretical functions was tested by comparing the EXAFS results obtained with the model compound β-$Cd(OH)_2$. Figure 2 compares the experimental and theoretical Cd-O and Cd-Cd EXAFS contributions for β-$Cd(OH)_2$. The use of McKale's functions and the Fourier-filtering routine (FITEX) resulted in six O atoms at 2.33 Å and six Cd atoms at 3.51 Å (Table 3). Spectral fitting using EXCURV resulted in six O atoms at 2.29 Å and six Cd atoms at 3.50 Å. Coordination numbers are accurate to ~10%, as are Debye-Waller factors listed in Table 3. Interatomic distances differ from crystallographic values by only a few hundredths of an angstrom. The precision of the evaluation of interatomic distances is 0.01 Å with both methods for the Cd shell but varies from 0.01 Å (McKale's functions) to 0.03 Å (EXCURV) for the O shell, differences that may derive from single-shell fitting in comparison with multiple-shell fitting. Because each approach has its merits, we employed both in analyzing the EXAFS of synthetic and natural apatites.

TABLE 3. Comparison of Cd-O and Cd-Cd distances in β-$Cd(OH)_2$ determined by X-ray diffraction and EXAFS

Atom (X)	CN	$R_{Crystall.}$* d(Cd-X) (Å)	FITEX** d(Cd-X) (Å)	FITEX** σ (Å)	EXCURV92† d(Cd-X) (Å)	EXCURV92† σ (Å)
O	6	2.32	2.33	0.08	2.29	0.08
Cd	6	3.50	3.51	0.10	3.50	0.09

Note: CN = coordination number.
* Wyckoff (1971).
** The EXAFS analysis was performed using McKale's phase-shift and amplitude functions.
† The calculation of phase-shift and amplitude functions was performed using Hedin-Lundqvist (Hedin and Lundqvist 1969) exchange potential.

RESULTS AND INTERPRETATION

Synthetic phosphate samples

Qualitative analysis. Despite the poorer signal-to-noise ratio of the $k^3\chi(k)$ spectrum R3, its shape is similar to that of R2 (Fig. 3). These two spectra are clearly different from R1; the frequencies are slightly different at low k, and the main spectral features are dissimilar. The three synthetic apatites differ mainly in Cd contents. In sample R1, Cd atoms are surrounded by other Cd atoms, whereas they can be, in principle, surrounded by Ca, Cd, or both in the two other samples depending on the distribution of Cd in the apatitic framework. If Cd atoms were segregated in clusters in samples R2 and R3, their spectra would be similar to that of R1. This simple comparison of the three reference spectra indicates that Cd atoms do not form clusters within the apatite structure of diluted references but are actually well dispersed at the atomic scale.

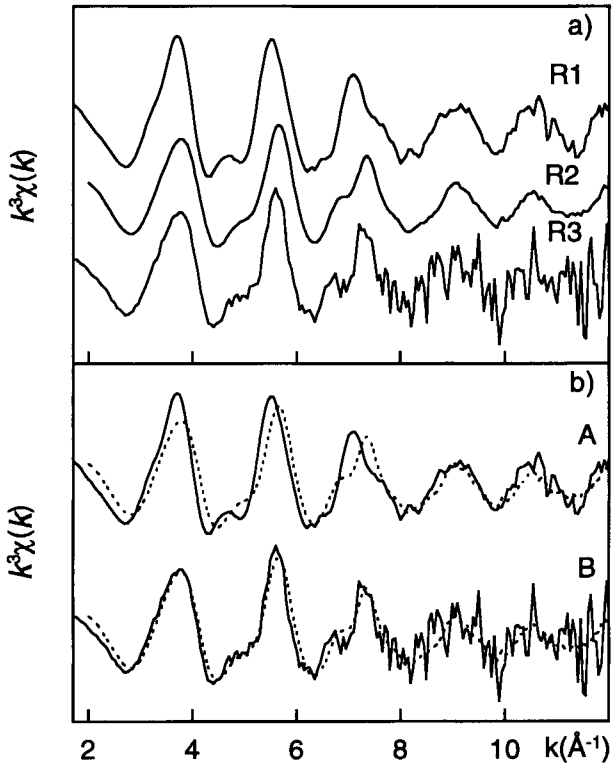

FIGURE 3. The k^3-weighted Cd K-edge EXAFS spectra for synthetic apatite samples: (**a**) individual spectra, (**b**) comparison of the various spectra. A = comparison of R1 (solid line) and R2 (dashed line) spectra. B = comparison of R2 (dashed line) and R3 (solid line) spectra.

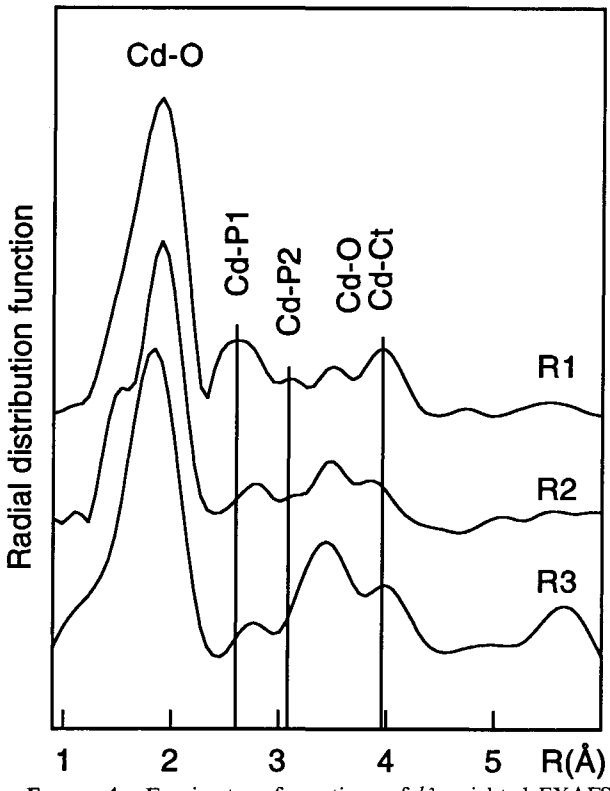

FIGURE 4. Fourier transformations of k^3-weighted EXAFS spectra for synthetic apatite samples. Radial distribution functions were not corrected for phase shift; accordingly, RDF peaks are shifted toward shorter distances by ~0.3–0.4 Å with respect to crystallographic values. Real distances obtained from least-squares fits are reported in Table 4.

Quantitative analysis. The $k^3\chi(k)$ spectra were Fourier-transformed over the 3.5–12 Å^{-1} k range to produce the RDFs with five main peaks (Fig. 4). On the basis of crystallographic data (Table 2), these peaks are attributed, with increasing distances, to Cd-O, Cd-P1, Cd-P2, Cd-O, and Cd-Ct (Ct = Cd or Ca) contributions. Because the apatite structure is common to R1, R2, and R3, the relative intensity of the various peaks necessarily depends on Cd concentration. In particular, we note a small but systematic increase in next-nearest-neighbor distances as Cd concentration decreases (Fig. 4).

The results obtained using McKale's functions are presented first, then the results obtained using the rapid curved-wave theory are presented. For the use of McKale's functions, first RDF peaks were Fourier filtered and analyzed with a single-shell model. For all samples,

TABLE 4. Structural parameters determined by EXAFS using McKale's functions (FITEX) and the rapid curved-wave theory with calculated phase-shift and amplitude functions (EXCURV92)

	FITEX*				EXCURV92**			Diffraction	
Atom (X)	⟨*R*⟩ (Å)	⟨CN⟩†	σ (Å)	τ (Å^{-2})‡	⟨*R*⟩ (Å)	⟨CN⟩§	σ (Å)	⟨*R*⟩ (Å)	⟨CN⟩‖
				R1 [$Cd_{10}(PO_4)_6(OH)_2$]					
O	2.33	6.6	0.10	2.0	2.28	6.6	0.10	2.40	6.6
O	—	—	—	—	—	—	—	2.76	2.2
P1	3.13	1.8	0.13	1.9	3.07	1.8	0.10	3.16	1.8
Cd	—	—	—	—	—	—	—	3.33	0.8
P2	3.45	3.0	0.14	1.9	3.45	3.0	0.16	3.47	3.0
O	3.93	5.4	0.09	2.0	3.91	5.4	0.07	3.95	5.4
Cd	3.95	8.4	0.15	1.3	3.93	8.4	0.13	3.98	8.4
O	—	—	—	—	—	—	—	4.38	4.8
				R2 [$Ca_{9.5}Cd_{0.5}(PO_4)_6(OH)_2$]					
O	2.30	6.0	0.11	2.0	2.26	6.0	0.10		
P1	3.11	1.5	0.14	1.9	3.07	1.5	0.11		
P2	3.47	3.4	0.16	1.9	3.44	3.4	0.18		
Ca	4.00	9.0	0.17	1.8	3.97	9.0	0.13		
O	4.35	7.0	0.13	2.0	4.03	7.0	0.10		
				R3 [$Ca_{9.995}Cd_{0.005}(PO_4)_6(OH)_2$]					
O	2.32	6.0	0.11	2.0	2.27	6.0	0.11		
P1	3.39	0.8	0.07	1.9	3.11	0.8	0.14		
P2	3.63	3.0	0.12	1.9	3.63	3.0	0.19		
Ca	4.05	9.8	0.16	1.8	4.02	9.8	0.14		

Note: CN is the coordination number, and σ is the Debye-Waller factor.

* In the FITEX program, the deviation (ΔE_0) from the threshold energy taken at $\Delta\mu/2$ was refined but held identical for each atomic shell: $\Delta E_0 = 9.2$ eV for R1, $\Delta E_0 = 10.6$ eV for R2, and $\Delta E_0 = 6.7$ eV for R3.

** In the EXCURV program, the Fermi energy E_F was defined: $E_F = -4.4$ eV for R1, $E_F = -9.0$ eV for R2, and $E_F = -8.8$ eV for R3.

† Values held fixed, equal to averaged crystallographic values, during the spectral fitting of R1 and refined for R2 and R3.

‡ The parameter τ is related to the mean free path of the electron, λ, by the relation $\lambda = k/\tau$. The value λ was determined for each atom type for sample R1 and was held fixed for samples R2 and R3. The value of λ for Ca is between the values determined for P and Cd, proportional to the atomic number.

§ Values held fixed, equal to values determined using McKale's functions, during the spectral fitting.

‖ Averaged coordination numbers. After crystallographic data of Hata et al. (1978).

least-squares fits indicate approximately 6–6.6 O atoms at 2.30–2.33 Å (Table 4). Peaks corresponding to Cd-P1, Cd-P2, and Cd-Ct contributions were backtransformed together because of the distance-related overlap of the various contributions. Because EXAFS spectroscopy provides only a weighted average in cases in which several crystallographic sites exist, average coordination numbers and interatomic distances were calculated for the Cd–end-member hydroxylapatite (R1) by applying a weighted linear combination of the values determined for Ct1 and Ct2 sites by X-ray diffraction (Table 4) (Hata et al. 1978). The weights correspond to the relative proportion of the Ct1 and Ct2 sites within the unit cell (four for Ct1 and six for Ct2) (Harries et al. 1986). For example, the Cd atom is surrounded at long distances by six Cd atoms at 3.95 Å in site 1 and ten Cd atoms at 4.00 Å in site 2. The weighted linear combination of these two shells results in an averaged shell of 8.4 [$(6 \times 4 + 10 \times 6)/10 = 8.4$] Cd atoms at the weighted distance of 3.98 Å. The contributions to the EXAFS signal of the second O shell, which contains 2.2 O atoms at the average distance of 2.76 Å, and the short-distance Cd shell, which contains 0.8 Cd atoms at 3.33 Å, are very weak, resulting from indirectly bound neighbors. To limit the number of free parameters in the fitting procedure ($N_{indep.} < 2\Delta k \Delta R/\pi$, where Δk is the k range for the spectral fitting, and ΔR is the width of the backtransform window), these two shells were omitted in the following study. Fitting trials for next-nearest neighbors were performed using a four-shell model: P1, P2, O, and Cd. Interatomic distances and Debye-Waller factors were refined for each shell, but coordination numbers were held constant and equal to the averaged crystallographic values. There were nine free parameters, which is thus below $N_{indep.} = 12$ in this case. The experimental and theoretical curves for the backtransformed first O and Ct shells of sample R1 are shown in Figure 5a, and the structural parameters obtained with this four-shell model are listed in Table 4. Least-squares fitting resulted in two P shells at 3.13 and 3.45 Å, one O shell at 3.93 Å, and one Cd shell at 3.95 Å.

The least-squares fitting of samples R2 and R3 used the same coordination numbers as for R1 as a starting point, but it was found necessary to replace Cd backscatterer atoms by Ca. For sample R2, the least-squares fit led to two P shells at 3.11 and 3.47 Å, one Ca shell at 4.00 Å, and one O shell at 4.35 Å (Table 4, Fig. 5a). In the case of sample R3, because of the high dilution (600 ppm), the EXAFS signal became very noisy for $k > 10$ Å^{-1} and $N_{indep.} = 9$. Accordingly, the number of adjustable shells was reduced to three. The three-shell model obtained for R3 was composed of two P shells at 3.39 and 3.63 Å and one Ca shell at 4.05 Å (Table 4, Fig. 5a).

The three spectra for the synthetic samples were also analyzed using the rapid curved-wave approximation.

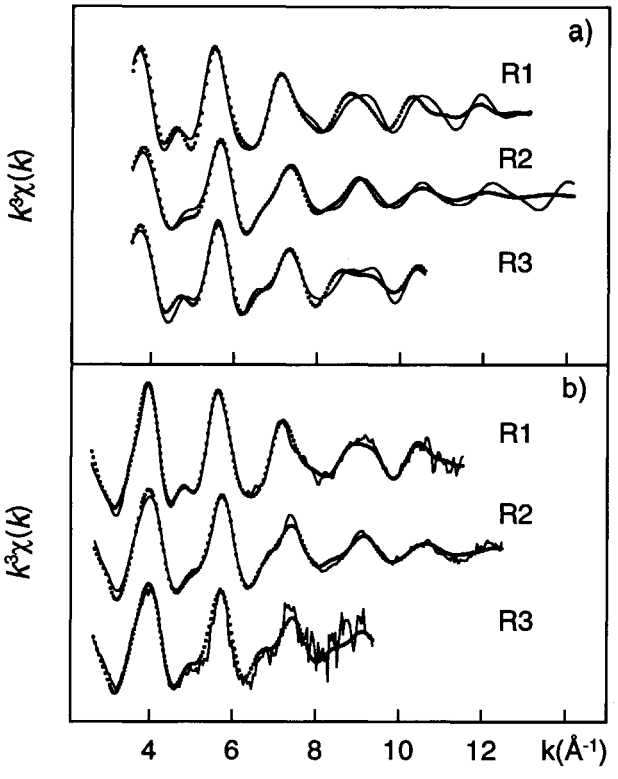

FIGURE 5. (a) Fourier-filtered Cd-O, Cd-P, and Cd-(Cd,Ca) contributions to EXAFS for synthetic apatites (solid lines) fitted with theoretical spectra (dotted lines) using McKale's functions. (b) Whole EXAFS spectra for synthetic apatites (solid lines) fitted with theoretical spectra (dotted lines) using the rapid curved-wave theory.

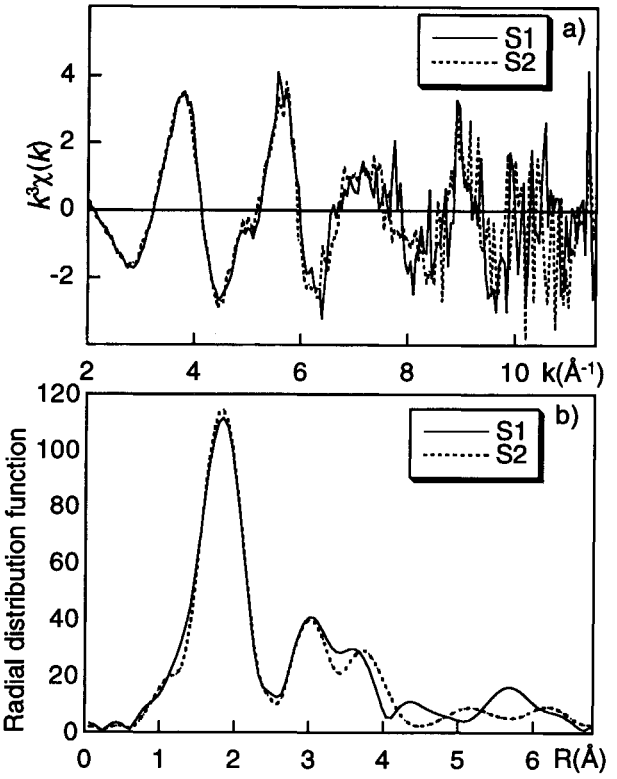

FIGURE 6. (a) The k^3-weighted Cd K-edge EXAFS spectra for natural apatites. (b) Radial distribution functions (RDFs) produced by Fourier transformation of EXAFS spectra over the 3.6–10 Å^{-1} k range (uncorrected for phase shift). EXAFS spectra and RDFs for the two samples have very similar line shapes.

Whole EXAFS spectra were fitted to all O and Ct shells at the same time, and the structural models employed the same coordination numbers determined by the previous FITEX analyses for each sample. Experimental and theoretical $k^3\chi(k)$ curves for each synthetic sample are presented in Figure 5b, and structural parameters are reported in Table 4. Examination of these parameters shows that interatomic distances determined by EXCURV are comparable to those obtained with McKale's functions, although O and Ct distances are marginally shorter, as we found in analyzing β-Cd(OH)$_2$ (Table 3).

From Table 4 it is clear that agreement, in the Cd environment, between EXAFS and X-ray diffraction (weighted Cd1 and Cd2 sites) in Cd–end-member hydroxylapatite is good, with all five main neighboring shells quantitatively differentiated. O nearest neighbors, however, are significantly shorter using either method of EXAFS analysis in comparison with crystallographic values, which may indicate a non-Gaussian distribution of the elementary Cd-O distances (Teo 1986).

The distances of the two P shells in sample R2 are comparable to those in sample R1, meaning that Cd atoms in sample R2 occupy both crystallographic sites in similar proportions as in Cd–end-member hydroxylapatite. The increase in the distances of P shells for sample R3 in comparison with samples R1 and R2 allows us to infer that the proportion of Ct1 sites occupied by Cd atoms in this sample is greater than in samples R1 and R2 (Tables 2 and 4). Cd atoms may preferentially occupy the Ct1 site at a very low substitution rate (0.005 atom per unit cell) in synthetic hydroxylapatite. The reverse trend was observed at a high substitution rate (0.5 atom per unit cell; Nounah et al. 1992; Jeanjean et al. 1994).

Natural samples

Qualitative analysis. EXAFS spectra and RDFs for the two natural samples are shown in Figure 6. The signal-to-noise ratio is good up to the k value of ~10 Å^{-1}, which reflects the reliability of the measurements at these very low concentrations of Cd. The spectral likeness indicates that Cd atoms in both samples have a similar atomic environment and that the mechanical and chemical treatments of the ores did not alter this environment.

The two spectra possess a clear beat pattern at ~4.7 Å^{-1}, which points to the existence of multiple frequencies and, therefore, to the presence of more than one atomic shell around Cd. To determine the location of Cd atoms at the atomic scale, these EXAFS spectra were compared with those of reference materials. In Figure 7, the EXAFS

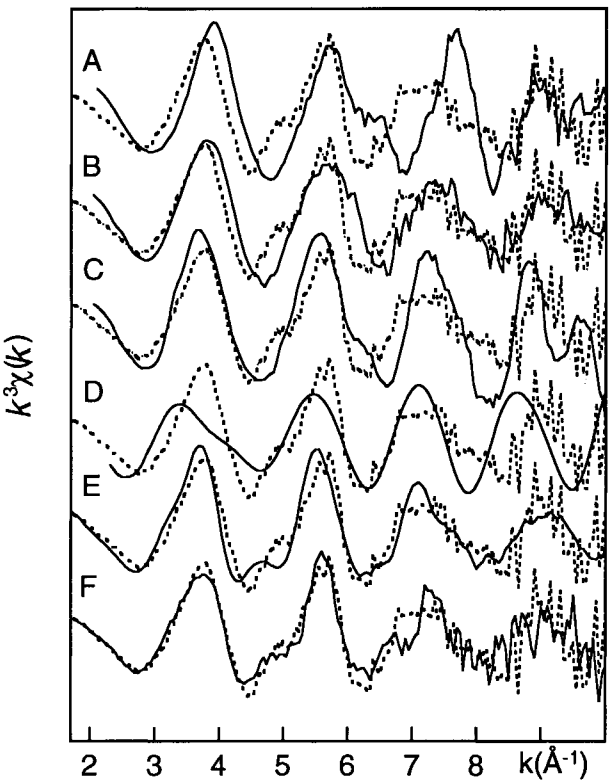

FIGURE 7. Comparison of the k^3-weighted Cd K-edge EXAFS spectrum for the natural apatite ore S2 (dotted lines) and those for various reference compounds (solid lines): (A) goethite coprecipitated with Cd (after Spadini et al. 1994), (B) Cd-adsorbed goethite (11% surface loading) (after Spadini et al. 1994), (C) otavite ($CdCO_3$), (D) Cd-containing crandallite (theoretical spectrum), (E) synthetic sample R1, and (F) synthetic sample R3.

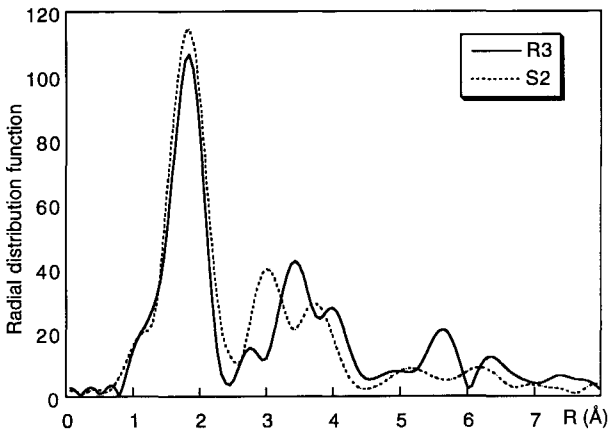

FIGURE 8. Comparison of RDFs (uncorrected for phase shift) for the natural apatite ore S2 (dotted line) and the synthetic apatite R3 (solid line). Note that the amplitudes of the second and third RDF peaks are similar but are shifted toward shorter distances for S2. This similarity of the amplitudes indicates that Cd atoms are located within the apatite structure and not at the grain surface or at grain boundaries.

spectrum for S2 (the most concentrated in Cd) is superimposed on the EXAFS spectra for Cd-containing and Cd-sorbed goethite (Spadini et al. 1994), $CdCO_3$ (otavite), Cd-containing crandallite, Cd–end-member hydroxylapatite (R1), and Cd-containing hydroxylapatite (R3) [in the absence of a crandallite sample, its EXAFS spectrum (D) was calculated from crystallographic data (Blount 1974) and by replacing Ca with Cd as the central atom]. The salient point of these comparisons is the close similarity of R3 and S2 spectra. The only apparent difference is the shift to high k values of the shoulder at 7 Å^{-1} for S2 (Fig. 7). This qualitative analysis proves that the majority of Cd is located within the apatitic structure of the phosphate ore.

Quantitative analysis. RDFs for the two natural samples, S1 and S2, are in close agreement with one another (Fig. 6) and provide real-space information regarding the similarity of the Cd environment in both apatite ore samples and their distinction with respect to synthetic apatites. The RDFs of S2 and of the synthetic hydroxylapatite containing a small amount of Cd (R3) are shown in Figure 8. Real-space structure beyond the nearest-neighbor O peak for S2 is shifted toward slightly shorter distances relative to those of R3. Nevertheless, this structure of next-nearest neighbors in the RDF for sample S2 is of the apatite local structure; the first peak being assigned to P neighbors and the second to Ca neighbors.

The fitting procedure was initially performed for natural samples S1 and S2 using McKale's functions. The least-squares fit of the backtransform of the first RDF peak led to six O atoms at 2.33 Å for sample S2 (Table 5). A minimum of three shells were necessary to obtain a good fit for the subsequent structure (Fig. 9), yielding two P shells at 3.17 and 3.52 Å and one Ca shell at 4.04 Å for S2 (Table 5). Note that this structural model reproduces the beat pattern at ~7.7 Å^{-1} rather well. In the rapid curved-wave analyses, coordination numbers were held constant to values corresponding to the average of both crystallographic site environments (Table 4). Examination of Table 5 shows that structural parameters derived from the EXCURV analysis are in good agreement with those determined using McKale's functions.

Although Cd-Ca distances determined for the natural samples are similar to those for dilute synthetic apatite (R3), Cd-P distances are shorter (Fig. 8), with d(Cd-P1) = 3.17 Å and d(Cd-P2) = 3.52 Å for S2, and d(Cd-P1) = 3.39 Å and d(Cd-P2) = 3.63 Å for R3. This shortening of the two Cd-P subshells in natural fluorapatite in comparison with synthetic hydroxylapatite accounts for the difference in their EXAFS wave frequency near 7 Å^{-1} (Fig. 7). We note from Table 2 that Cd-P distances are shorter for site 2 than for site 1, suggesting that Cd in the apatite ores preferentially occupies Ct2 sites. Note that these sites contain bonded F.

DISCUSSION

The possible presence of a secondary Cd-bearing mineral admixed with apatite was investigated by attempting

TABLE 5. Comparison of structural parameters of samples S1 and S2 determined using McKale's functions (FITEX) and the rapid curved-wave theory (EXCURV92)

Atom (X)	S1							S2						
	FITEX*				EXCURV92**			FITEX*				EXCURV92**		
	R (Å)	CN†	σ (Å)	τ (Å^{-2})	R (Å)	CN‡	σ (Å)	R (Å)	CN†	σ (Å)	τ (Å^{-2})	R (Å)	CN‡	σ (Å)
O	2.32	7.0	0.11	2.0	2.27	6.6	0.10	2.33	7.0	0.11	2.0	2.28	6.6	0.10
P1	3.17	0.6	0.08	1.9	3.18	1.8	0.08	3.17	1.1	0.10	1.9	3.18	1.8	0.10
P2	3.53	3.0	0.12	1.9	3.48	3.0	0.08	3.52	3.1	0.12	1.9	3.49	3.0	0.09
Ca	4.02	9.0	0.14	1.8	4.01	8.4	0.14	4.04	7.0	0.14	1.8	4.02	8.4	0.15

Note: CN is the coordination number, and σ is the Debye-Waller factor.
* The value ΔE_0 = 8.2 eV for S1 and 7.7 eV for S2 (FITEX).
** E_F = −10.8 eV for S1 and −10.7 eV for S2 (EXCURV92).
† Values refined during the spectral fitting.
‡ Values held fixed, equal to the values determined for each atomic shell for sample R1, during the spectral fitting.

linear decompositions of S2 with R2, R3, Cd-containing goethite, and otavite EXAFS spectra. Attempts to reproduce precisely the natural apatite spectrum over the whole k range, and specifically the distinctive structure at 7 Å^{-1}, were unsuccessful. On the basis of the close resemblance of the spectra of R3 and the natural samples, the maximum percentage of Cd possibly located outside the apatite is believed to be <20%, if any.

The fact that the amplitudes of the second and third RDF peaks for the natural samples and R3 are comparable indicates that Cd atoms are located in the apatitic framework and not adsorbed at the mineral surface or at a grain boundary. Moreover, the structural parameters obtained for Cd atoms enable us to assess that Cd substitutes for Ca on both crystallographic sites and is not located in interstitial sites (i.e., in apatite channels). The decrease in distance of the Cd-P correlation peaks for natural apatite in comparison with R3 (Fig. 8) can be interpreted by assuming that the proportion of Ca2 sites occupied by Cd is greater for natural fluorapatite samples than for the synthetic hydroxylapatite sample R3, although the amount of Cd in each compound is about the same (0.005 Cd atom for R3 and 0.001 Cd atom for the natural samples, per unit cell). Sorption experiments have shown that dissolved Cd^{2+} may easily diffuse into channel in apatite and then substitute for Ca in the Ca2 site, which is located in the vicinity of channels (M. Fedoroff, personal communication). The partitioning of Cd into the Ca2 site of natural apatites, in comparison with the coprecipitated reference samples, suggests that the source of some of the Cd in this phosphate ore was the circulation of Cd-containing fluids.

The substitution of Cd for Ca in the apatite structure implies that the process of extraction of Cd from phosphate ores must include a calcination or a dissolution stage to break the apatitic framework for liberating Cd.

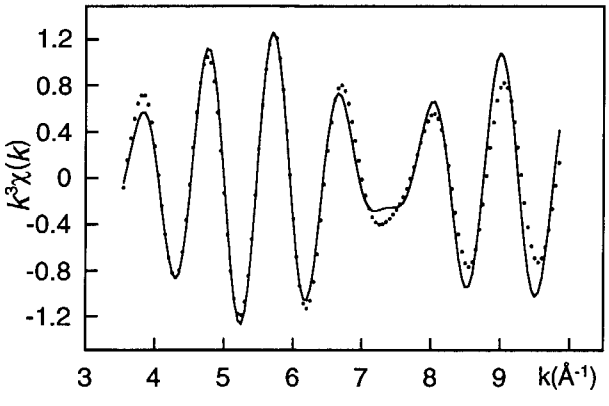

FIGURE 9. Fourier-filtered Cd-P and Cd-Ca contributions to EXAFS (solid line) and theoretical spectrum (dotted line) for natural sample S2 obtained using McKale's functions.

ACKNOWLEDGMENTS

The authors gratefully thank A. Nounah for providing synthetic apatite samples and Daresbury Laboratory for providing access to the beam. A.S. thanks the EEC for a fellowship.

REFERENCES CITED

Beevers, C.A., and McIntyre, D.B. (1945) The atomic structure of fluorapatite and its relation to that of tooth and bone material. Mineralogical Magazine, 27, 254–257.

Blount, A.M. (1974) The crystal structure of crandallite. American Mineralogist, 59, 41–47.

Brès, E.F., Cherns, D., Vincent, R., and Morniroli, J.P. (1993) Space-group determination of human tooth-enamel crystals. Acta Crystallographica B, 49, 56–62.

de Boo, W. (1990) Cadmium in agriculture. Toxicological and Environmental Chemistry, 27, 55–63.

Gurman, S.J., Binsted, N., and Ross, I. (1984) A rapid, exact curved-wave theory for EXAFS calculations. Journal of Physics C: Solid State Physics, 17, 143–151.

Harries, J.E., Hukins, D.W.L., and Hasnain, S.S. (1986) Analysis of the EXAFS spectrum of hydroxylapatite. Journal of Physics C: Solid State Physics, 19, 6859–6872.

Hata, M., Okada, K., Iwai, S., Akao, M., and Aoki, H. (1978) Cadmium hydroxylapatite. Acta Crystallographica, B34, 3062–3064.

Hedin, L., and Lundqvist, S. (1969) Effects of electron-electron and electron-phonon interactions on the one-electron states of solids. Solid State Physics, 23, 1–181.

Hutton, M. (1983) Sources of cadmium in the environment. Ecotoxicology and Environmental Safety, 9–24.

Jeanjean, J., Vincent, U., and Fedoroff, M. (1994) Structural modification of calcium hydroxylapatite induced by sorption of cadmium ions. Journal of Solid State Chemistry, 108, 68–72.

Kay, M.I., Young, R.A., and Posner, A.S. (1964) Crystal structure of hydroxylapatite. Nature, 204, 1050–1052.

Koningsberger, D.C., and Prins, R. (1988) X-ray absorption: Principles, applications, techniques of EXAFS, SEXAFS and XANES, 673 p. Wiley, New York.

Lee, P.A., and Pendry, J.B. (1975) Theory of the extended X-ray absorption fine structure. Physics Review B, 11, 2795–2811.

Mackie, P.E., and Young, R.A. (1973) Location of Nd dopant in fluorapatite, $Ca_5(PO_4)_3F$:Nd. Journal of Applied Crystallography, 6, 26–31.

Manceau, A., and Combes, J.M. (1988) Structure of Mn and Fe oxides and oxyhydroxides: A topological approach by EXAFS. Physics and Chemistry of Minerals, 15, 283–295.

McKale, A.G., Veal, B.W., Paulikas, A.P., Chan, S.K., and Knapp, G.S. (1988) Improved ab initio calculations for extended absorption fine structure spectroscopy. Journal of the American Chemical Society, 110, 3763–3768.

Mortvedt, J.J., and Osborn, G. (1982) Studies on the chemical form of cadmium contaminants in phosphate fertilizers. Soil Science, 134, 185–192.

Nounah, A., Szilagyi, J., and Lacout, J.L. (1990) La substitution calcium-cadmium dans les hydroxylapatites. Annales de Chimie Française, 15, 409–419.

Nounah, A., Lacout, J.L., and Savariault, J.M. (1992) Localization of cadmium in cadmium-containing hydroxy- and fluorapatites. Journal of Alloys and Compounds, 188, 141–146.

Nriagu, J.O. (1980) Cadmium in the environment, 363 p. Wiley, New York.

Spadini, L., Manceau, A., Schindler, P.W., and Charlet, L. (1994) Structure and stability of Cd^{2+} surface complexes on ferric oxides: I. Results from EXAFS spectroscopy. Journal of Colloid and Interface Science, 168, 73–86.

Stipp, S.L., Hochella, M.F., Parks, G.A., and Leckie, J.O. (1992) Cd^{2+} uptake by calcite, solid-state diffusion, and the formation of solid-solution: Interface processes observed with near-surface sensitive techniques (XPS, LEED, and AES). Geochimica et Cosmochimica Acta, 56, 1941–1954.

Sudarsanan, K., and Young, R.A. (1969) Significant precision in crystal structural details: Holly Springs hydroxylapatite. Acta Crystallographica, B25, 1534–1543.

Teo, B.K. (1986) EXAFS: Basic principles and data analysis, 349 p. Springer-Verlag, Berlin.

Thomas, V., and Spiro, T. (1994) Emissions and exposure to metals: Cadmium and lead. In R. Socolow, C. Andrews, F. Berkhout and V. Thomas, Eds., Industrial ecology and global change, p. 297–320. Cambridge University Press, Cambridge.

Williams, C.H. (1974) Heavy metals and other elements in fertilizers: Environmental considerations. In D.R. Leece, Ed., Fertilizers and the environment, p. 123–150. N.S.W. Branch, Australian Institut of Agricultural Science, Sydney.

Williams, C.H., and David, D.J. (1976) The accumulation in soil of cadmium residues from phosphate fertilizers and their effect on the cadmium content of plants. Soil Science, 121, 86–93.

Wyckoff, R.W.G. (1971) Crystal structures, vols. 1–6, Wiley, New York.

Manuscript received April 6, 1995
Manuscript accepted March 7, 1996